JOURNAL OF THERMOPHYSICS AND HEAT TRANSFER
Vol. 28, No. 2, April–June 2014

Porous-Material Analysis Toolbox Based on OpenFOAM and Applications

Jean Lachaud*
University of California, Santa Cruz, Santa Cruz, California 95064
and
Nagi N. Mansour†
NASA Ames Research Center, Mountain View, California 94035

DOI: 10.2514/1.T4262

The Porous-material Analysis Toolbox based on OpenFOAM is a fully portable OpenFOAM library. It is implemented to test innovative multiscale physics-based models for reacting porous materials that undergo recession. Current developments are focused on ablative materials. The ablative material response module implemented in the Porous-material Analysis Toolbox relies on an original high-fidelity ablation model. The governing equations are volume-averaged forms of the conservation equations for gas mass, gas species, solid mass, gas momentum, and total energy. It may also simply be used as a state-of-the-art ablation model when the right model options are chosen. As applications, three physical analyses are presented: 1) volume-averaged study of the oxidation of a carbon-fiber preform under dry air, 2) three-dimensional analysis of the pyrolysis gas flow in a porous ablative material sample facing an arcjet, and 3) comparison of a state-of-the-art and a high-fidelity model for the thermal and chemical response of a carbon/phenolic ablative material.

Downloaded by AIAA on August 11, 2014 | http://arc.aiaa.org | DOI: 10.2514/1.T4262

Nomenclature

A_i	=	gaseous species i
A_j	=	Arrhenius law pre-exponential factor, SI
C_H	=	Stanton number for heat transfer
C_M	=	Stanton number for mass transfer
c_p	=	specific heat, $\mathrm{J \cdot kg^{-1} \cdot K^{-1}}$
e	=	specific energy, $\mathrm{J \cdot kg^{-1}}$
E_j	=	Arrhenius law activation energy, $\mathrm{J \cdot kg^{-1}}$
$\mathcal{F}_i$	=	diffusion flux of the ith species, $\mathrm{kg \cdot m^{-2} \cdot s^{-1}}$
F_j	=	fraction of mass lost through pyrolysis reaction j
Fo	=	Forchheimer number
h	=	specific enthalpy, $\mathrm{J \cdot kg^{-1}}$
j	=	diffusive flux, $\mathrm{mol \cdot m^{-2} \cdot s^{-1}}$
K	=	permeability
K_i	=	chemical equilibrium constant for reaction i
l	=	thickness or length, m
M_k	=	molar mass of species k, $\mathrm{kg \cdot mol^{-1}}$
m_j	=	Arrhenius law parameter
$\dot{m}$	=	mass flow rate, $\mathrm{kg \cdot m^{-2} \cdot s^{-1}}$
N_g	=	number of gaseous species
N_p	=	number of pyrolysis reactions
n_j	=	Arrhenius law parameter
p	=	pressure, Pa
q	=	heat flux, $\mathrm{J \cdot m^{-2} \cdot s^{-1}}$
R	=	perfect gas constant, $\mathrm{J \cdot kg^{-1} \cdot K^{-1}}$
$\underline{\underline{\mathbf{T}}}$	=	second-order tensor
$\boldsymbol{u}$	=	vector
v	=	convection velocity, $\mathrm{m \cdot s^{-1}}$
y	=	mass fraction
β	=	Klinkenberg coefficient, Pa
γ_{ji}	=	stoichiometric coefficient, reaction j species i
μ	=	viscosity, $\mathrm{Pa \cdot s^1}$
ξ_j	=	advancement of pyrolysis reaction j
ε	=	volume fraction
$\prod$	=	pyrolysis gas production rate, $\mathrm{kg \cdot m^{-3} \cdot s^{-1}}$
π	=	molar pyrolysis gas production rate of species i, $\mathrm{mol \cdot m^{-3} \cdot s^{-1}}$
ρ	=	density, $\mathrm{kg \cdot m^{-3}}$.
τ	=	characteristic time, s
τ^s	=	mechanical erosion rate, $\mathrm{mol \cdot m^{-3} \cdot s^{-1}}$
ω	=	reaction rate, $\mathrm{mol \cdot m^{-3} \cdot s^{-1}}$
ω^s	=	solid reaction rate, $\mathrm{mol \cdot m^{-3} \cdot s^{-1}}$

Subscripts

a	=	ablative material (gas, fiber, and matrix)
c	=	char
e	=	boundary layer edge properties
f	=	reinforcement (non-pyrolyzing phase)
g	=	gas phase
m, PM	=	pyrolyzing material
mv	=	virgin polymer matrix
p	=	pyrolysis
pg	=	pyrolysis gas
s	=	solid phase

I. Introduction

A POROUS-MATERIAL Analysis Toolbox based on OpenFOAM (PATO) is being developed as a fully portable OpenFOAM library. OpenFOAM is an open-source finite volume computational fluid dynamic (CFD) software released by OpenCFD Limited.[‡] OpenFOAM and PATO are implemented in the C++ programming language. They are supported for Unix/Linux operating systems.

PATO is a modular analysis platform specifically implemented to test innovative physics-based models for reactive porous materials submitted to high-temperature environments. The governing

Presented as Paper 2013-2767 at the 44th AIAA Thermophysics Conference, San Diego, CA, 24–27 June 2013; received 25 August 2013; revision received 30 November 2013; accepted for publication 3 December 2013; published online 27 May 2014. This material is declared a work of the U.S. Government and is not subject to copyright protection in the United States. Copies of this paper may be made for personal or internal use, on condition that the copier pay the $10.00 per-copy fee to the Copyright Clearance Center, Inc., 222 Rosewood Drive, Danvers, MA 01923; include the code 1533-6808/14 and $10.00 in correspondence with the CCC.

*Scientist, SVI/UCSC, NASA Ames Research Park, Building 19, Moffett Field; jlachaud@ucsc.edu. Senior Member AIAA.

†Chief Scientist for Modeling and Simulation, TN Division, Building 254, Moffett Field; nagi.n.mansour@nasa.gov. Associate Fellow AIAA.

‡The PATO library is not endorsed by OpenCFD Limited, the producer of the OpenFOAM software and owner of the OPENFOAM® and OpenCFD® trademarks. www.openfoam.org/ [retrieved 21 January 2014].

equations implemented in the different modules are volume-averaged forms of the conservation equations for porous media. Although PATO could be used to model any porous material, it is currently developed more specifically for ablative materials. PATO inherits the flexibility and versatility of OpenFOAM, making it an excellent platform to 1) easily and reliably implement and test new models, 2) down-select models/mathematical frameworks prior to implementing them in production codes, and 3) analyze special configurations and conditions not readily available in production codes.

The objective of this article is to describe an original high-fidelity ablation model, its modular implementation in PATO, and several concrete applications and physical analyses. In Sec. II, we give an overview of the phenomenology of porous ablative materials. In Sec. III, the volume-averaged mathematical framework for ablative porous materials implemented in PATO is presented. This framework is fully compatible with current state-of-the-art ablation models but adds new models specific to porous media. In Sec. IV, PATO itself is presented: modules available, numerical method, and verification. Then, three original applications/analyses that bring insight on the behavior of porous ablative material are proposed.

II. Phenomenology of Porous Ablative Materials

To illustrate the modeling section, Fig. 1 puts in perspective in a single chart the following illustrations.

First, a macroscopic illustration (center) shows the response of low-density carbon/phenolic ablative materials during atmospheric entry. The virgin material undergoes thermal degradation and ultimately recession captured by the following physicochemical phenomena [1]: solid pyrolysis, pyrolysis gas transport and chemistry, and ablation chemistry. In the pyrolysis-zone, the phenolic polymer is thermally decomposed and progressively carbonized into a low-density turbostratic graphite, losing mass while releasing pyrolysis gases under the form of water, hydrogen, and hydrocarbons [2–4]. To illustrate this process without getting into too much detail in this overview, the production of hydrogen and phenol that are two principal products of the pyrolysis are shown in the illustration. Phenol (C_6H_5OH) is schematically represented by a white carbon cycle with an OH group. In the coking and ablation zones, the pyrolysis gases released by solid pyrolysis percolate and diffuse to the surface through the network of pores. Reactions within the pyrolysis gas mixture (homogeneous reactions, e.g., $C_6H_5OH + H_2 \leftrightharpoons C_6H_6 + H_2O$) and between pyrolysis gases and the char take place with possible coking effects (heterogeneous reactions, e.g., $C_6H_6 \leftrightharpoons C_{6(gr)} + 3H_2$). Mixing and possible reaction of the pyrolysis gases with boundary layer gases into the pores of the material occur when boundary layer gases penetrate the material by forced convection or due to fast diffusion at low pressures. In the ablation zone, the material is removed by ablation and the initial surface recedes. Depending on entry conditions, ablation may be caused by heterogeneous chemical reactions (oxidation, e.g., $2C_{(gr)} + O_2 \leftrightharpoons 2CO$, or sometimes nitridation), phase change (sublimation, e.g., $C_{(gr)} \leftrightharpoons C_{(gas)}$), and possibly mechanical erosion (often called spallation). For porous materials, the thickness of the ablation zone depends on the thermochemical conditions and the material microstructure [5].

Second, a microscopic illustration (right) shows the microscopic (fiber-scale) architecture of the virgin material and its evolution with charring and ablation. The images are scanning electron microscopy (SEM) scans and direct numerical simulations (DNS) at the fiber scale [6]. The microscopic scale simulations are extremely costly in computational time (typically 24 h on a single processor to simulate the oxidation of a 400 μm × 100 μm × 100 μm carbon preform during 1 s [6]) and cannot realistically be used for design or thermal protection system (TPS) response analysis. The fundamental microscopic-scale equations need to be volume-averaged [7] into

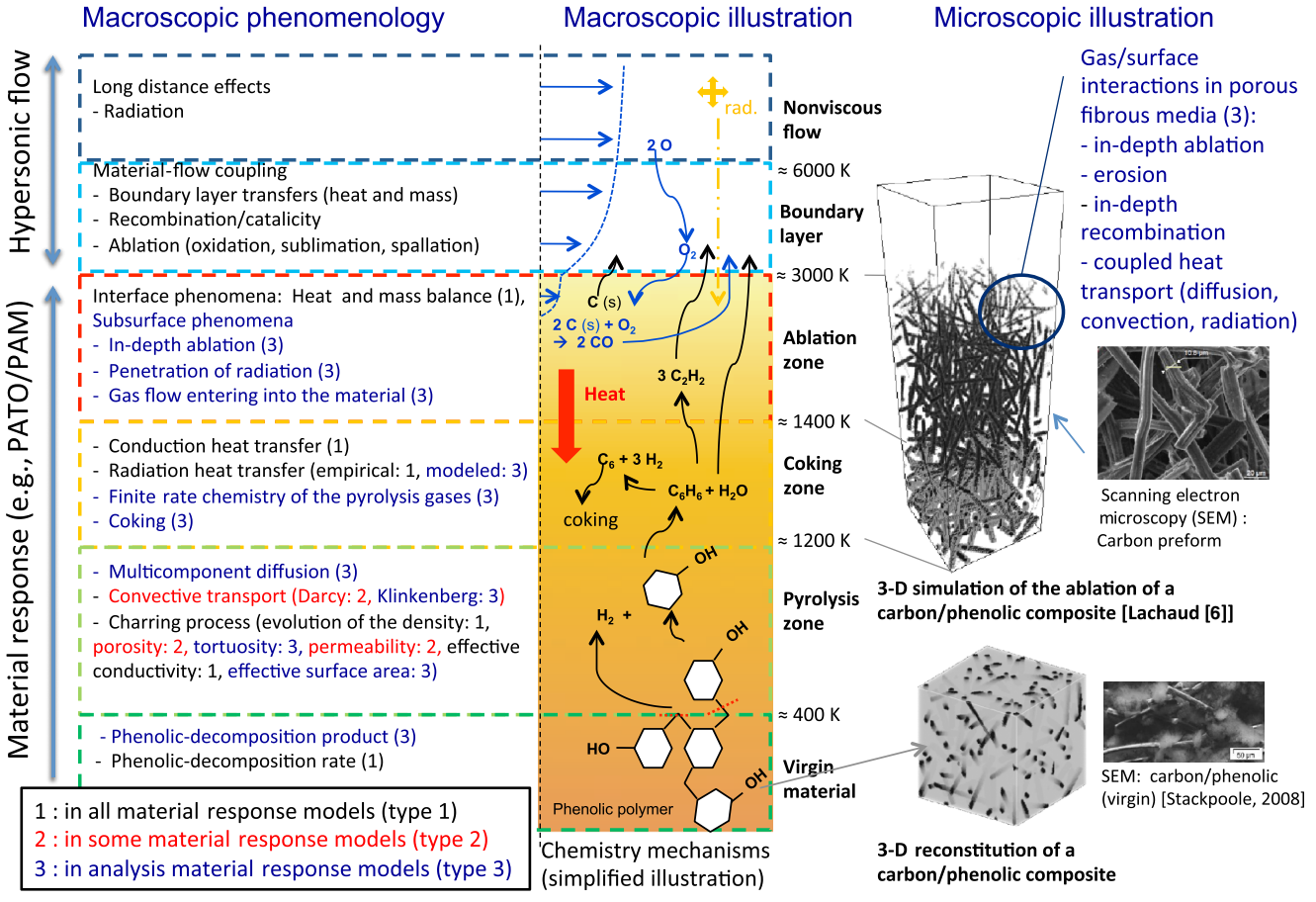

Fig. 1 Illustration of the phenomenology of porous ablative materials (a low-density carbon/phenolic ablative material is used as an example).

Downloaded by AIAA on August 11, 2014 | http://arc.aiaa.org | DOI: 10.2514/1.T4262

physics-based macroscopic equations that can be solved more efficiently [8]. PATO includes a suite of tools that can be used to extract intrinsic (microscopic) data (e.g., fiber reactivity) from macroscopic experiments and to guide the development of volume-averaged models [6].

Third, a macroscopic summary of the phenomenology (left side of the figure) using the common macroscopic-scale (volume-averaged) nomenclature for the mass, momentum, and energy conservation terms is shown. A review of the models published in the open literature reveals three levels of coherent models [9]. A complete description, in equations, is available in Sec. IV but we wish to provide a quick overview here. The first level, based on the state-of-the-art Charring Material Ablation (CMA) [1] model, is implemented in all design codes; its phenomenology is referenced as type 1. The core phenomena of the pyrolysis-ablation problem are modeled but many simplifications are used. A major simplification is that the momentum conservation is not implemented, meaning that the direction of the pyrolysis flux and the internal pressure need to be arbitrarily prescribed by the user. This type 1 model is well adapted for unidimensional, quasi-steady-state, and equilibrium or frozen chemistry conditions. The second level includes the implementation of the momentum conservation. This capability is found in a few design codes and in several recent analysis codes [9]. The added terms are referenced as type 2. Referenced as type 3 are the details of the physical phenomena occurring in a porous carbon/phenolic ablative material. Three-dimensional (3-D) type 2 and type 3 solvers are available in PATO.

III. Volume-Averaged Mathematical Framework for Porous Ablative Materials

This section presents a mathematical framework for porous ablative materials. The governing macroscopic equations to model porous media are volume-averaged forms of the mass, momentum, and energy conservation equations [7]. Current type 1 and 2 state-of-the-art models are based on simplified derivations of these three fundamental equations [9,10]. We present here an exact volume-averaged [7] derivation for a type 3 model and its associated boundary conditions. The proposed mathematical framework has directly been developed for type 3 models but degenerates in state-of-the-art type 1 and type 2 models under the same physical hypotheses. This layered structure presents a remarkable advantage because new modules can easily and rigorously be compared to heritage models, as shown in Sec. V.

The presentation of this section can be followed in parallel in Fig. 1. We will continue using low-density carbon/phenolic as an example. In other words, we will assume that the material is made of three phases: carbon fibers, phenolic polymer, and gas (in the pores).

A. Mass Conservation

The gaseous mass-conservation equation includes a production term (right-hand side) to account for the pyrolysis gas production, noted Π, and reads

$$\partial_t(\varepsilon_g\rho_g) + \partial_x \cdot (\varepsilon_g\rho_g \boldsymbol{v}_g) = \Pi \tag{1}$$

In all type 1 and in some type 2 codes [9], the time derivative is omitted and the gas flow problem is treated as a succession of steady-state problems. This simplification is acceptable when the variations of the intensive variables (temperature, pressure) are slow compared to the characteristic time of the flow in the porous medium [9]. The determination of the direction of the gas velocity, v_g, is necessary to solve the average mass conservation equation. In type 1 codes, this equation is numerically integrated with the assumption that the gas flow is perpendicular to the surface and directed toward the surface. This is correct for one-dimensional (1-D) steady-state problems with an impermeable back face; in other configurations, the direction and velocity of the flow has to be determined by resolution of the momentum conservation equation (see Sec. III.B). The pyrolysis gas production Π is traditionally obtained by fitting thermogravimetry analysis of the resin decomposition using one or several Arrhenius laws [11]. For example, for phenolic polymers, it has been shown that the pyrolysis degradation process follows four steps [3], which may be described by four heterogeneous decomposition reactions [4]. Therefore, for any pyrolyzing phase within a given ablative material, a convenient notation for $j \in [1, N_p]$ pyrolysis reactions is

$$\mathrm{PM}_j \rightarrow \sum_{i=1}^{N_g} \gamma_{ji} A_i \tag{2}$$

where PM_j is a fictive solid species of the pyrolyzing material, which is the phenolic matrix in the case of low-density carbon/phenolic. The pyrolyzing phase density is given by

$$\varepsilon_m\rho_m = \varepsilon_{mv}\rho_{mv} \sum_{j=1}^{N_p} F_j(1-\xi_j) \tag{3}$$

where

$$\frac{\partial_t \xi_j}{(1-\xi_j)^{m_j}} = T^{n_j}\mathcal{A}_j \exp\left(-\frac{E_j}{\mathcal{R}T}\right) \tag{4}$$

The pyrolysis-gas production is given by

$$\Pi = -\partial_t(\varepsilon_m\rho_m) = \varepsilon_{\mathrm{mv}}\rho_{\mathrm{mv}} \sum_{j=1}^{N_p} F_j \partial_t(\xi_j) \tag{5}$$

In the literature, the form of the equations used to describe pyrolysis vary but they are all mathematically equivalent. State-of-the-art design codes (type 1 and 2) do not track species production. Only the average mass production Π is computed from the Arrhenius laws. A constant elemental fraction of the pyrolysis gas is assumed. This is known to not be fully correct because the composition of the gases produced by pyrolysis is not constant — it is a function of temperature, heating rate, and possibly pressure [4,12]. The gas chemical composition and derived quantities (gas enthalpy, viscosity, mean molar mass) are computed assuming chemical equilibrium in general (type 1 and type 2 codes). This assumption is often correct, but sometimes leads to a pyrolysis reaction model that is exothermic instead of endothermic, as experimentally observed [13]. Heuristic methods that arbitrarily modify the enthalpy of the pyrolysis gases to obtain a better agreement with experimental observations have been proposed [14]. In this case, the actual gas composition and other properties (viscosity, mean molar mass, diffusion coefficients) are still unknown because the real gas composition is unknown. This is not a problem for type 1 codes, which completely ignore these terms. However, the arbitrary modification of the pyrolysis gas enthalpy (without tracking the real gas composition) creates an inconsistency in type 2 codes that make use of the viscosity and mean molar mass to compute the gas flow direction and the internal pressure. Therefore, for high-fidelity modeling, it is important to experimentally determine not only the elemental composition of the pyrolysis gases, but also their molar composition. The pyrolysis gas production rate for each species i is obtained using

$$\pi_i = \varepsilon_m\rho_{\mathrm{mv}} \sum_{j=1}^{N_p} [\partial_t \xi_j F_j \tilde{\gamma}_{ji}] \tag{6}$$

where

$$\tilde{\gamma}_{ji} = \frac{\gamma_{ji}}{\sum_{k=1}^{N_g} \gamma_{jk}\mathcal{M}_k} \tag{7}$$

This requires the experimental determination of the stoichiometric factors γ_{ji}, which are not directly available in the literature but may be derived from experimental studies [2–4]. For type 1 and type 2 models, the overall pyrolysis gas production may still be obtained from the same data set by summing over the production terms $\Pi = \sum_{i=1}^{N_s} [\pi_i M_i]$. Obviously, some quality information is lost during the summing process, but this shows well the compatibility between

Downloaded by AIAA on August 11, 2014 | http://arc.aiaa.org | DOI: 10.2514/1.T4262

type 1, 2, and 3 models and how code users can always switch back to the simplest models when in possession of type 3 data.

Type 3 models include the species conservation equation to accurately track species transport and chemical reactions within the pores of the material. The species conservation equation may be written in mass fraction y_i as

$$\partial_t(\varepsilon_g\rho_g y_i) + \partial_x \cdot (\varepsilon_g\rho_g y_i v_g) + \partial_x \cdot \mathcal{F}_i = \pi_i M_i + \varepsilon_g \omega_i M_i \quad (8)$$

where $\mathcal{F}_i$ is the diffusion flux of the ith species. At low pressures, mass transfer (diffusion) in porous media is not negligible compared to convection [5]. Multicomponent mass transfer in porous media is a complex problem that we treat in two steps. First, the average bulk diffusion coefficients is computed for each species. Then, the Bosanquet model [5] is used in a second step to account for tortuosity effects in all regimes (Knudsen to continuum). There currently is no reliable, or even well founded, finite rate chemistry model for the homogeneous and heterogeneous reactions of pyrolysis gases ω_i. In Sec. V, we use a coherent model based on the reduction of a large combustion database [15], but its validation for ablative materials is still in process.

A solid phase mass conservation model is implemented in all models to compute the effective density of the solid. The volume-averaged density change of the matrix due to pyrolysis Π is modeled using forms equivalent to

$$\partial_t(\varepsilon_m\rho_m) = -\Pi \quad (9)$$

Coking is completely neglected in type 1 and 2 codes. Ablation and spallation are modeled as surface phenomena, so they do not appear in in-depth equations. In the proposed type 3 framework, the solid mass conservation equation is generalized to account for in-depth heterogeneous reactions (coking, ablation [8]) and spallation

$$\partial_t(\varepsilon_s\rho_s) = \partial_t(\varepsilon_m\rho_m + \varepsilon_f\rho_f) = -\Pi + \sum_{i\in s}\varepsilon_g\omega_i M_i + \sum_{i\in s}\tau_i M_i \quad (10)$$

This overall mass balance is valid for any material. The determination of the intrinsic heterogeneous reaction rates for ablation and coking $\omega_{i,i\in s}$ is not an easy task. The in-depth ablation and coking behaviors of the different phases depend on the microstructure of the material of interest. An original experimental technique and a modeling approach have been proposed to extract the needed parameters [8]. There are two technical difficulties: 1) measuring the intrinsic reaction rates at the fiber scale [16] and 2) modeling the microstructure and its evolution due to ablation and coking [17]. The first application of Sec. V shows how PATO may be used to extract such parameters from a simple oxidation experiments.

B. Momentum Conservation in Porous Media

In type 2 and 3 codes, the average gas velocity is obtained by resolution of the momentum conservation equation. In porous media, the volume-averaged momentum conservation may be written as

$$v_g = -\frac{1}{\varepsilon_g\mu}\frac{1+\beta/p}{1+Fo}\underline{\underline{\mathbf{K}}} \cdot \partial_x p \quad (11)$$

Most of the materials are anisotropic; therefore, the permeability $\underline{\underline{\mathbf{K}}}$ is a second-order tensor. For example, FiberForm, the carbon preform of the Phenolic Impregrated Carbon Ablator (PICA) [18], has orthotropic permeability properties [19]. For creeping Stokes flows in the continuum regime (in the pores of the material), the momentum conservation degenerates into Darcy's law ($\beta = 0$, $Fo = 0$). The term $1 + \beta/p$ is the Klinkenberg correction to account for slip effects at the pore scale when the Knudsen number (ratio of the mean free path to the mean pore diameter) is not small. The term $1 + Fo$ is the Forchheimer correction to account for high-velocity effects at the pore scale (flow separation in the continuum regime). Typically, Forchheimer effects are expected to occur for pyrolysis gas velocities higher than 50 m/s (that is, in high-density ablative materials submitted to very high heat fluxes). It is not advised to use both corrections simultaneously as they address different regimes.

C. Energy Conservation

According to Puiroux et al. [20], solid and gas phases are in thermal equilibrium as long as the Péclet number for diffusion of heat within the pores is small ($Pe = \epsilon_g\rho_g c_{p,g} d_p v_g/k_g$). In most applications of interest for space agencies, the small pore size (<100 μm) and the slow pyrolysis gas flow ($v_g \sim 1$ m/s) ensure a small Peclet number: the gas temperature accommodates to the solid temperature within the pores [5]. Under the thermal equilibrium assumption, the energy conservation may be written as

$$\partial_t(\rho_a e_a) + \partial_x \cdot (\varepsilon_g\rho_g h_g \boldsymbol{v}_g) + \partial_x \cdot \sum_{i=1}^{N_g}(h_i \boldsymbol{\mathcal{F}}_i) = \partial_x \cdot (\underline{\underline{\mathbf{k}}} \cdot \partial_x T) + \mu\varepsilon_g^2(\underline{\underline{\mathbf{K}}}^{-1} \cdot \boldsymbol{v}) \cdot \boldsymbol{v} \quad (12)$$

where the total storage energy of the ablative material is the sum of the energy of its phases

$$\rho_a e_a = \varepsilon_g\rho_g e_g + \varepsilon_m\rho_m h_m + \varepsilon_f\rho_f h_f \quad (13)$$

The second and third terms of the left-hand side are the energy convected (advection) and the energy transferred (diffusion) by the pyrolysis gases, respectively. Heat transfer is conveniently modeled as an effective diffusive transfer (Fourier's law). The effective conductivity $\underline{\mathbf{k}}$ is a second-order tensor accounting for conduction in the solid, conduction in the gas, and effective radiative heat transfer. The validity of this approach is questionable. The main issue is the validity of the linearization of the radiative heat transfer. A theoretical study has shown that radiative heat transfer may be linearized for two-dimensional (2-D) carbon fiber preforms [21,22]. The applicability to other materials and the experimental validation are not straightforward and need to be investigated, but this is outside the scope of this presentation. The second term on the right-hand side is the energy dissipated by viscous effects in Darcian regime [23]. It is, in general, small compared to the heat transfer term.

It may seem that no major improvement is added to the momentum and energy conservation equations in type 3 models, but they actually inherit the detailed resolution of the mass conservation equations because the following parameters are now computed with more accuracy: viscosity, mean molar mass, porosity, permeability, and enthalpies.

D. Boundary Conditions

At the bondline, conservative boundary conditions are generally used (adiabatic and impermeable). At the surface, simple wall boundary conditions may be used for simple analyses. A popular condition consists of prescribing temperature, pressure, and recession (they can change as a function of time). It is not described here because it is trivial but it is available in PATO and most codes. In ablative conditions, when the wall temperature and the surface recession are unknown, surface energy balance and surface mass balance are used as boundary conditions. This is presented next.

1. Surface Energy Balance

The surface energy balance at the wall depicted in Fig. 2 reads

$$q_{\text{conv}} - (\rho V)h_w + q_{\text{rad,in}} - q_{\text{rad,out}} - q_{\text{cond}} + \dot{m}_{\text{pg}}h_{\text{pg}} + \dot{m}_{\text{ca}}h_{\text{ca}} = 0 \quad (14)$$

where the convective heat flux [$q_{\text{conv}} = \rho_e u_e C'_H(h_e - h_w)$] and the radiative heat flux are extracted from CFD simulations. The Stanton number C_H is corrected to account for the blockage induced by the pyrolysis-ablation gas blowing; that is, the heat transfer coefficient is corrected. For example, the following correction is widely used $C'_H = C_H \ln(1 + 2\lambda B')/\ln(2\lambda B')$, where $B' = (\dot{m}_{\text{pg}} + \dot{m}_{\text{ca}})/(\rho_e u_e C_M)$ is a dimensionless mass flow rate and λ is a scaling factor

Downloaded by AIAA on August 11, 2014 | http://arc.aiaa.org | DOI: 10.2514/1.T4262

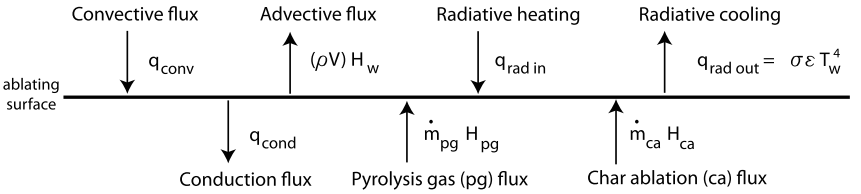

Fig. 2 Energy balance at the wall.

usually taken equal to 0.5 [24]. The resolution of Eq. (14) requires the evaluation of the pyrolysis gas flow rate $\dot{m}_{pg}$ and of the ablation rate $\dot{m}_{ca}$.

2. Surface Mass Balance and Recession Rate

The pyrolysis gas flow rate $\dot{m}_{pg}$ is directly obtained in the material response code by integration of the pyrolysis, transport, and mass equations, as explained previously. However, the ablation rate $\dot{m}_{ca}$ is a function of both the mass transfer in the boundary layer and the thermochemical properties at the wall (pyrolysis gas blowing rate and composition, temperature, pressure, and boundary layer gas composition). A common practice is to assume thermochemical equilibrium at the wall to compute the ablation rate. The model still in use in the community was developed in the 1960s [25]. It is based on element conservation in steady state in a control volume close to the wall, as sketched in Fig. 3 and expressed in Eq. (15). The underlying hypothesis is that over a time increment Δt, the equilibrium chemistry problem in the control volume is quasi steady (decoupling of the material response and of the boundary layer problem). This increment Δt should be at least as long as the time increment of the heat transfer simulation (material response code), but short enough so that p, T, $\dot{m}_{pg}$, and y_{pg} variations may be neglected. This is verified in typical applications. For this presentation, we shall assume equal diffusion coefficients of the elements. Failure modes (spallation, mechanical erosion) are not included and the char is assumed to be composed of a single element (for example, carbon).

The inputs and outputs to this problem are as follows.

1) Inputs: $\dot{m}_{pg}$, $y_{k,pg}$, $y_{k,ca} = 1$, $y_{k,e}$, p, T.

2) Outputs: $\dot{m}_{ca}$, $y_{k,w}$.

The conservation of the mass fraction of element k in the control volume close to the wall reads

$$j_{k,w} + (\rho V) y_{k,w} = \dot{m}_{pg} y_{k,pg} + \dot{m}_{ca} y_{k,ca} \tag{15}$$

where pg represents pyrolysis gases, ca represents char ablation products, and w represents wall (or control volume). The usual element conservation rules apply:

1) The relative mass fractions sum to 1 in each phase

$$\sum_k y_{k,w} = 1; \qquad \sum_k y_{k,pg} = 1; \qquad \sum_k y_{k,ca} = 1$$

2) Because p and T are fixed, the element mass fraction conservation in the control volume is equivalent to the mass conservation.

Under the hypotheses that Prandtl = Lewis = 1 and that the diffusion coefficients are equal for the elements, Eq. (15) may be rewritten as

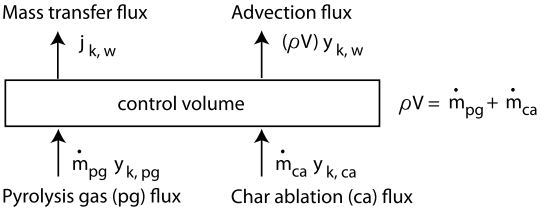

Fig. 3 Element mass fraction conservation at the wall.

$$\rho_e u_e C_H (y_{k,w} - y_{k,e}) + (\rho V) y_{k,w} = \dot{m}_{pg} y_{k,pg} + \dot{m}_{ca} y_{k,ca} \tag{16}$$

where C_H is the Stanton number and $(\rho V) = \dot{m}_{pg} + \dot{m}_{ca}$.

The formation reaction of species A_i may be written

$$A_i \rightleftharpoons \sum_{k \in \text{Elements}} \nu_{i,k} A_k \tag{17}$$

The i chemical equilibriums read

$$\sum_{k \in \text{Elements}} \nu_{i,k} \ln(x_k) - \ln(x_i) - \ln(K_i) = 0 \tag{18}$$

with $x_i = 1$ if A_i is a solid species. Species mole fractions sum to one

$$\sum_{i \in \text{Species}} x_i = 1 \tag{19}$$

The set of equations solved is

$$\rho_e u_e C_H (y_{k,w} - y_{k,e}) + (\rho V) y_{k,w} = \dot{m}_{pg} y_{k,pg} + \dot{m}_{ca} y_{k,ca} \tag{20}$$

$$\sum_{k \in \text{Elements}} \nu_{i,k} \ln(x_k) - \ln(x_i) - \ln(K_i) = 0 \tag{21}$$

with $x_i = 1$ if A_i is a solid species

$$\sum_{i \in \text{Species}} x_i = 1 \tag{22}$$

The base model may be extended when needed to account for multicomponent mass transfer, nonequal diffusion coefficients, failure (spallation, melting), a solid phase made of more than one element (example: SiO_2), and heterogeneous finite rate chemistry.

IV. Modules Available in PATO, Numerical Method, and Verification

PATO is composed of two types of modules, a global analysis module and an elementary analysis module, as shown in Table 1. The global analysis module may be used to run a full ablative material response with an applied/macroscopic scale point of view. The Pyrolysis–Ablation Module (PAM) module is an implementation of type 2 (PAM_2) and type 3 (PAM_3) material response models, as described in the previous section and summarized in Table 1. Any physically correct variation between these two models can be run when selecting the right model options. The elementary analysis module may be used to study specific fundamental aspects with a detailed/microscopic scale point of view. The Carbon Oxidation Analysis Code (COACO) module is specifically developed to analyze carbon oxidation experiments and extract intrinsic reaction rates of carbon fibers. It is also used to test and validate volume-averaged fiber oxidation models, needed for PAM_3, Eq. (10) [8].

PATO is a fully portable OpenFOAM extend library. OpenFOAM is an open-source finite volume CFD code. Therefore, PATO uses the finite volume method as well. To offer a more flexible modeling environment, equations are solved sequentially (as opposed to block-matrix resolution) at each time step. Each equation is solved implicitly and first-orders schemes (in time and space) are used by default, as they have been found to be sufficiently accurate. The schemes can, however, be modified by the user at run time whenever needed. This OpenFOAM functionality is inherited when using

Downloaded by AIAA on August 11, 2014 | http://arc.aiaa.org | DOI: 10.2514/1.T4262

Table 1 Summary of the capabilities of PATO's modules

	Global analysis modules		Elementary analysis modules	
PATO	PAM_2	PAM_3	COACO_1	COACO_2
Summary				
Model fidelity (1–3)	2	3	1	3
Code dimensionality (1–3)	3	3	1	3
Code maturity level (1–3)	3	1	3	1
Gas phase mass Conservation		**In-depth: Eq. (1)**		
Storage ($\partial_t \epsilon_g \rho_g$)	x	x		x
Divergence ($\partial_x \cdot (\epsilon_g \rho_g \boldsymbol{v}_g)$)	x	x		x
Pyrolysis production (Π)	x	x		
Pyrolysis model		**In-depth: Eq. (2–7)**		
State of the art Arrhenius laws (gives Π)	x	x		
Species production (gives πi)		x		
Gas-species conservation		**In-depth: Eq. (8)**		
Storage ($\partial_t \epsilon_g \rho_g y_i$)		x	x	x
Divergence ($\partial_x \cdot (\epsilon_g \rho_g y_i \boldsymbol{v}_g)$)		x	x	x
Diffusion ($\partial_x \boldsymbol{F}_i$)		x	binary	multicomponent
Pyrolysis species prod. ($\pi_i M_i$)		x		
Finite-rate chemistry ($\omega_i M_i$)		x	x	x
Solid-phase mass conservation		**In-depth: Eq. (9) and (10)**		
Pyrolyzing matrix mass loss	x	x		
In-depth ablation/coking		x	x	x
Momentum conservation		**In-depth: Eq. (11)**		
Darcy's law ($v_g = f(\partial_x p)$)	x	x		
Klinkenberg correction		x		
Energy conservation		**In-depth: Eq. (12) and (13)**		
Storage ($\partial_t \rho_a e_a$)	x	x		
Divergence ($\partial_x \cdot (\epsilon_g \rho_g h_g v_g)$)	x	x		
Diffusion ($\partial_x \cdot \Sigma(h_i F_i)$)	x	x		
Effective conduction (Δk)	x	x		
Viscous dissipation $f(K, v)$		x		
Boundary conditions		**At the wall: Eq. (14–22)**		
Prescribed pressure ($p(t)$)	x	x		
Prescribed temperature ($T(t)$)	x	x	x	x
Surface energy balance (Q)	x	x		
Boundary layer approx. (B')	x	x		
Fixed species concentration		x	x	x
Other utilities				
Equilibrium chemistry solver		Mutation++		
Gas properties		Mutation++		
Automatic mesh generation	1-D, 2-D IsoQ wedge, 3-D cylinder	1-D, 2-D IsoQ wedge, 3-D cylinder		

Table 2 Pyrolysis balance equations and kinetic parameters

j	Pyrolysis balance equations	Peak, K	F_j	A_j	E_j	m_j	n_j
	Model (Sykes [2]/Goldstein [11]/Trick [3,4])	S./T.	S.	G.	G.	G.	G.
1	$PM_1 \rightarrow H_2O$ (*physisorbed*)	373	0.01	$8.56 \cdot 10^3$	$7.12 \cdot 10^4$	3	0
2	$PM_2 \rightarrow 0.69H_2O + 0.01C_6H_6 + 0.01C_7H_8 + 0.23C_6H_6O$	773	0.24	$8.56 \cdot 10^3$	$7.12 \cdot 10^4$	3	0
3	$PM_3 \rightarrow 0.09CO_2 + 0.33CO + 0.58CH_4$	873	0.03	$4.98 \cdot 10^8$	$1.70 \cdot 10^5$	3	0
4	$PM_4 \rightarrow H_2$	1073	0.06	$4.98 \cdot 10^8$	$1.70 \cdot 10^5$	3	0
5	$PM_5 \rightarrow C$	—	0.66	0	0	3	0

sequential solvers. All well-known schemes up to the second-order are available in OpenFOAM. There are three benefits to the sequential approach that are very useful for an analysis toolbox: 1) each equation is easily modified without impacting the stability of the whole solver, 2) independent numerical schemes may be tested for each term of each equation at execution time, and 3) more equations can easily be added in the sequence to test new models. Mutation++, developed at the von Karman Institute[§] is used as a third-party library to compute all chemistry and transport related data, and for the surface mass balance in chemical equilibrium.

The individual verification of PATO operators is straightforward. OpenFOAM provides an extensive set of discretization algorithms and numerical schemes that are systematically verified by OpenCFD. However, it is still useful to verify that OpenFOAM modules are correctly used in PATO. Verifications of the time-dependent heat transfer and momentum equations have been carried out by comparison with analytical solutions and with a commercial CFD tool (FlexPDE).[¶] For the overall verification of the PAM modules, several ablation test cases have been specifically designed to allow rigorous material response code comparisons. The effort was started in 2011 to allow comparisons of ablative material response codes and models in an open forum. Since then, two test case series have been proposed within the framework of the NASA/AFOSR/SNL ablation

[§]Data available online at www.vki.ac.be/ [retrieved 21 January 2013].

[¶]Data available online at www.pdesolutions.com [retrieved 21 January 2014].

Downloaded by AIAA on August 11, 2014 | http://arc.aiaa.org | DOI: 10.2514/1.T4262

workshop each year [26,27]. In 2013, the third test case series was presented at the Gordon Research Conference on Atmospheric Entry [28]. The test case series are designed to propose problems of increasing complexity. Each series tackles only a few aspects of the material response to allow a targeted comparison of the codes and models. The first test case was mostly a heat transfer problem chosen for its simplicity, allowing focus on the in-depth material response [26]. The second test case series went one step further and made use of a convective boundary condition, as in state-of-the-art design codes [27]. The main goal of the third series is to test the 2-D axisymmetrical and 3-D modeling capabilities of the participating codes and assess multidimensional effects [28]. PATO was one of the codes used to design the three test case series, together with FIAT [24] (series 1), MOPAR [29] (series 1, 2), and Amaryllis [30] (series 2, 3). Extensive comparisons of PATO/PAM_2 with FIAT (series 1), MOPAR (series 1 and 2), and Amaryllis (series 1, 2) have been done with an excellent agreement. All test cases are included in the tutorials distributed with PATO releases. We present here a comparison for the most elaborated and well-defined test case at this time, which is test case 2.3. In summary, test case 2.3 consists in a 5 cm unidimensional sample of Theoretical Ablative Composite for Open Testing (TACOT) [26], heated on one side by a convective air heat flux at atmospheric pressure for 1 min followed by a cool down phase of 1 min. For a complete description of the test case please, refer to the test case description document [26]. Figure 4 shows the comparison between Amaryllis and PATO/PAM_2 for test case 2.3 in the format required in the test case description document [27]. It features thermocouple-type output on the top graph, and in the bottom graph the following: pyrolysis gas flux, ablation flux, location of the virgin/charring zone interface, location of the char/charring zone interface, and extend of recession. The agreement between PATO/PAM_2 and Amaryllis is excellent for all data.

V. Applications

Three analyses are presented to show the three main new features of the newly developed and implemented ablation model. The first

Downloaded by AIAA on August 11, 2014 | http://arc.aiaa.org | DOI: 10.2514/1.T4262

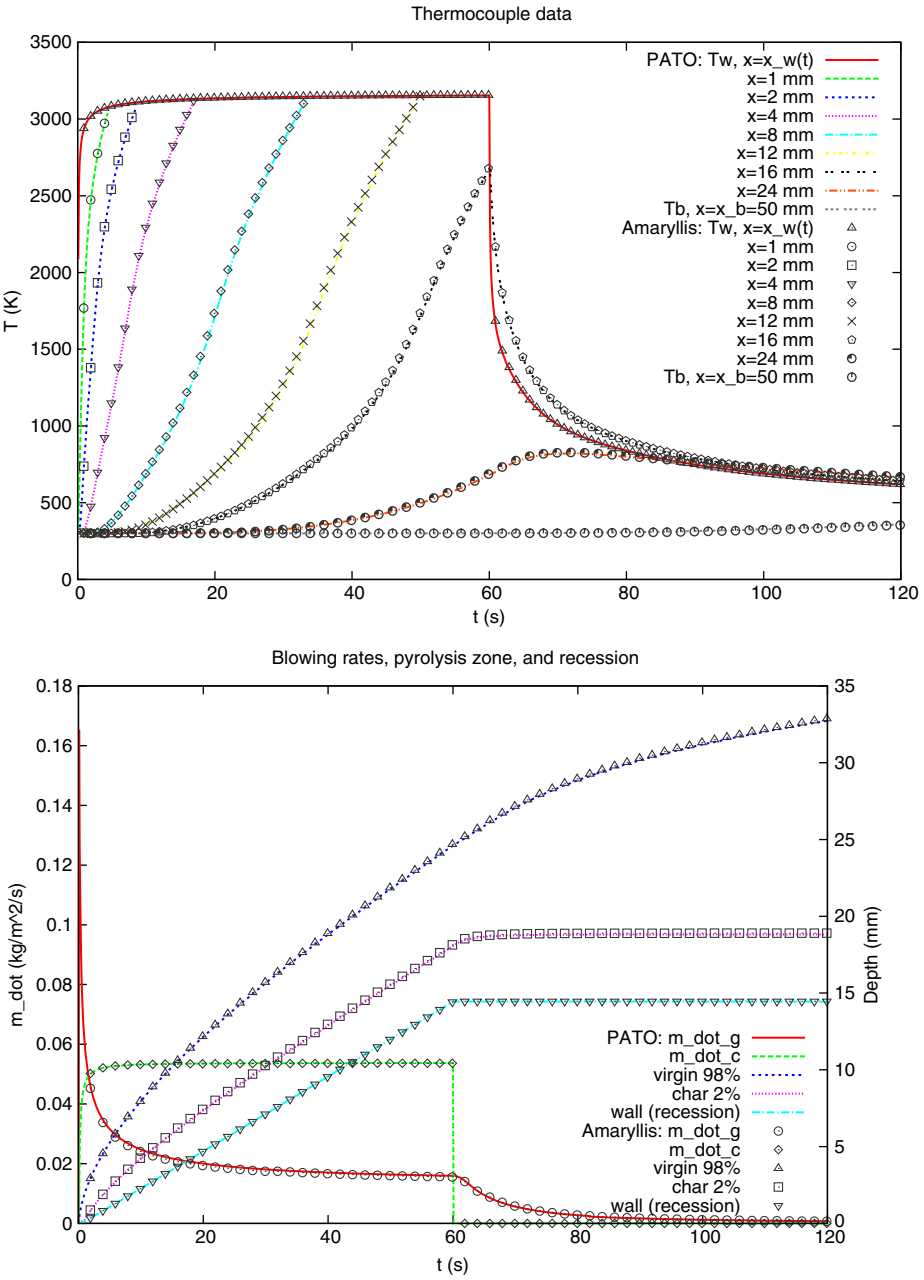

Fig. 4 Ablation test case 2.3: Comparison of PATO/PAM_2 and Amaryllis (type 2). It should be noted that the surface recedes past the five near-surface thermocouples. This is why the reading of these thermocouples is discontinued when they reach the surface temperature.

application aims at showing the ability of the high-fidelity model to capture the macroscopic scale behavior of carbon fiber materials using fiber-scale modeling. The objective is to illustrate how adding the averaged fiber-scale model to the state-of-the-art model helps to better capture the physics of in-depth ablation and brings invaluable insight when analyzing ablated samples.

The second application presented is a 3-D simulation of a porous ablative material cylinder facing an arcjet. A type 2 model is used to accurately compute the pyrolysis gas flow within the porous material (average momentum conservation, that is, Darcy's model). The objective is to analyze the pyrolysis gas flow direction and see the importance of correctly modeling gas flow in porous media to accurately account for multidimensionality effects.

The third application aims at comparing a type 2 and a type 3 ablation model for a low-density carbon/phenolic composite. A very simple test case is used to allow for an intuitive understanding of the differences observed between the numerical results. The focus is set on the analysis of finite rate chemistry effects.

A. Analysis of Oxidation of a Carbon Preform in a Flow Tube Reactor

The first application proposed has been presented in detail in [8]. We will summarize here the main findings and COACO results. Readers interested in more details are kindly asked to refer to the original publication. The objective of this work was to analyze the oxidation mechanism of a carbon fiber preform and obtain its effective reaction rate in order to provide data for Eq. (10) of type 3 models. The oxidation of FiberForm, an industrial carbon fiber preform, was studied in a tubular oxidation reactor at 898 K; dry air at 898 K and 1013 hPa was blown through a cylindrical plug interference-fit inside a quartz tube. The microscopic oxidation behavior of the fibers was analyzed by SEM after testing. The carbon fibers clearly oxidize via a progressive reduction of their diameter. The overall material recession occurs when the fibers are consumed. It was obvious that a reaction/diffusion-convection competition had driven the oxidation process and controlled the depth of oxidation (Fig. 5). Using COACO, it is possible to infer the intrinsic reactivity of the carbon fibers from the knowledge of the depth of oxidation. Indeed, because the diffusion coefficients are known variables, the only unknown in the reaction/diffusion competition problem is the intrinsic fiber reactivity, which controls the depth of oxidation. COACO results are shown in Fig. 6. The time-dependent simulation results show the evolution of the oxygen concentration in the reactor, the progressive reduction of the mean fiber radius, and the overall sample recession. In this simulation, the oxygen concentration drops quickly as the air flow enters into the carbon fiber preform. This happens because the oxydation rate is fairly high compared to the diffusion rate. The intrinsic reactivity of the carbon fibers has been found to be surprisingly high. This has been explained by the presence of calcium in the fibers. Calcium is know to be a catalyst in the oxidation of carbon fibers.

B. Analysis of Pyrolysis Gas Flow and Heat Transport in a 3-D Cylinder Facing an Arcjet

This example presents a purely theoretical case aiming at showing the 3-D capabilities of PATO and the interest of type 2 codes that can compute the direction of the pyrolysis gas flow. A cylinder of TACOT is heated for 40 s by a mini arcjet with a stagnation region that is small compared to the size of the sample. The cylinder has impermeable walls on the sides and bottom. The following conditions were arbitrarily chosen for the heat load at the stagnation point: 3 MW/m^2, recovery enthalpy $= 10$ MJ/kg, $p = 1013$ hPa, air, and a Gaussian decay was used along the radial direction. The case has been studied with PATO/PAM_2. We show and analyze results after 40 s of heating. Figures 7 and 8 show the ablation profile, the temperature and pressure contours, and the pyrolysis gas flow. A well-defined hot zone develops in the center of the sample. The internal pressure that builds up below the hot zone generates a fully multidimensional pyrolysis gas flow. A fraction of the pyrolysis gas goes down first and then escapes from outside the hot zone. Therefore, such a problem is typically not monodimensional, even in its center, and needs to be analyzed with a multidimensional code that models the gas flow direction (type 2 model).

C. Finite Rate Chemistry Effects on Temperature Profile and Gases Injected in the Boundary Layer

We propose here a simple application to show finite rate chemistry effects. We use as a support the ablation test case 1.0 [26] and compare type 1, type 2, and type 3 code results. Test case 1.0 is unidimensional. As shown in Fig. 9, a sample of TACOT of 5 cm is heated on one side at 1664 K for 1 min at atmospheric pressure and cooled down by reradiation for 1 min. Adiabatic boundary conditions are used at the bottom. The initial conditions are $p = 1$ atm (101,325 Pa), $T = 300$ K, and sample length: 0.05 m. The initial gas composition in the material is left open. We use pyrolysis gases at equilibrium for the type 2 model because this is the usual practice. We use dry air for the finite rate chemistry case because it makes more sense. The type 2 model used is the one presented in the ablation test case document and in the TACOT definition file [28]. We believe that the finite rate chemistry models initially proposed in the TACOT definition file can be significantly improved. Therefore, we use here what we think is a better set of data. The high-fidelity pyrolysis model provided in Table 2 and derived from literature data is used.

A reduced 22-species homogeneous finite rate chemistry mechanism, derived from the combustion database of Blanquart [15], is used for the homogenous chemistry of the pyrolysis gases. The first graph (Fig. 10) shows the excellent agreement between PATO/PAM_2 and FIAT (type 1), showing that in this simple configuration type 1 and type 2 codes provide similar results, as discussed in Sec. III. Figure 11 shows a comparison of the thermal response when using finite rate chemistry vs equilibrium chemistry. The difference is explained by the fact that the pyrolysis gas enthalpies are significantly different (equilibrium vs finite rate), as shown in Fig. 12.

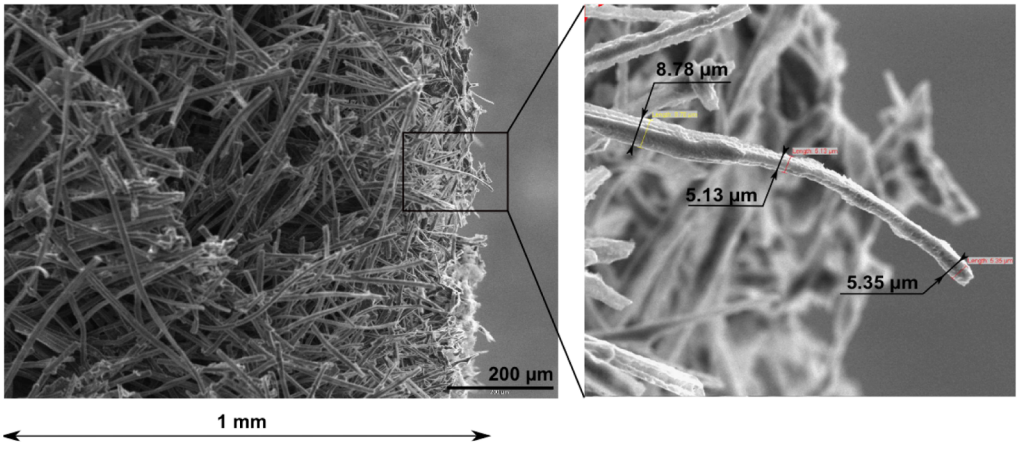

Fig. 5 SEM of the exposed side of the FiberForm cylinder. On this figure, the dry airflow (898 K, 1013 hPa) is from right to left.

Downloaded by AIAA on August 11, 2014 | http://arc.aiaa.org | DOI: 10.2514/1.T4262

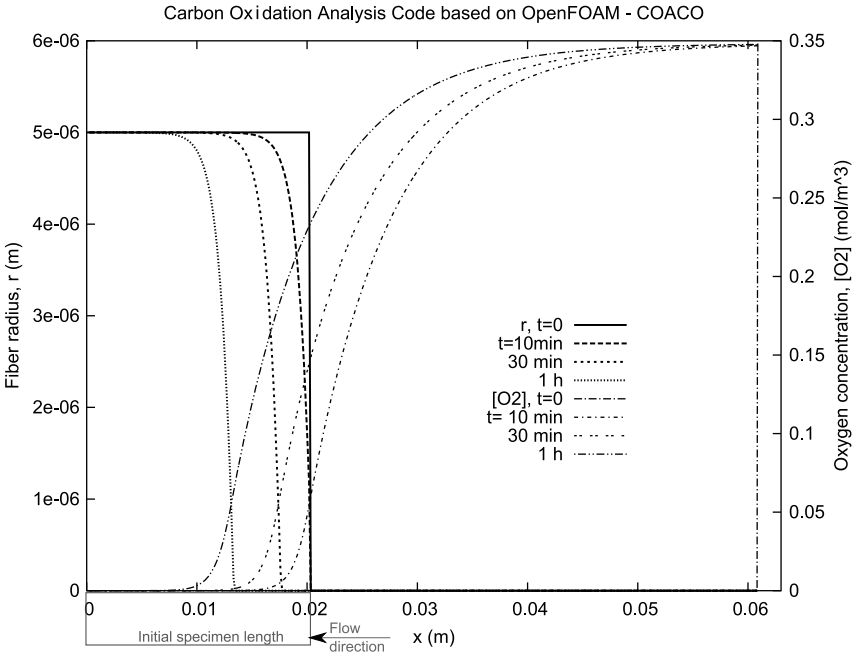

Fig. 6 COACO_1 simulation of the time-dependent oxidation of a carbon fiber preform used to extract the intrinsic reactivity of the carbon fibers.

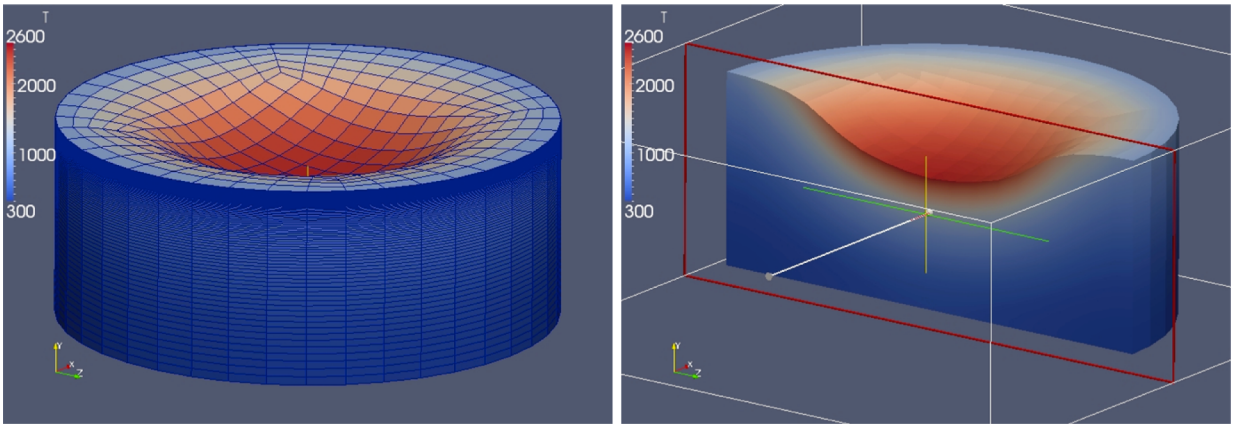

Fig. 7 PAM_2 temperature contour of a cylindrincal sample of TACOT under microarcjet conditions at 40 s.

Downloaded by AIAA on August 11, 2014 | http://arc.aiaa.org | DOI: 10.2514/1.T4262

Figure 13 shows the list of species considered in the 22-species model and evolution of the pyrolysis gas composition as it is convected through the material toward the surface, here in the absence of diffusion. It is obvious that in this case, the finite rate chemistry model used in the material will have a strong influence on the predicted species in the boundary layer and that the equilibrium assumption would not be correct. It is interesting to note that a large amount of benzene (A1) is injected in the boundary layer according to the finite rate chemistry model used, whereas benzene is not even present when using equilibrium chemistry.

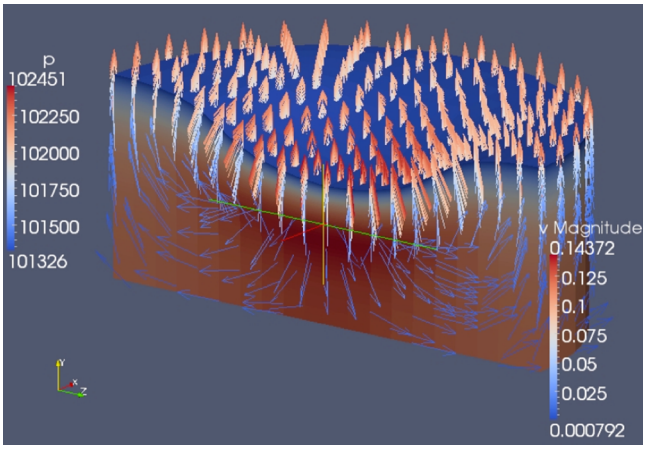

Fig. 8 PAM_2 pressure contour and pyrolysis gas veocity vectors for a cylindrincal sample of TACOT under microarcjet conditions at 40 s.

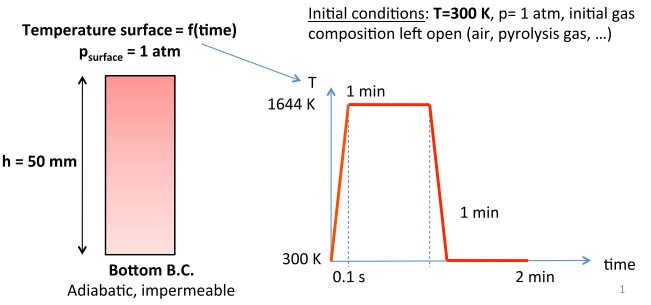

Fig. 9 Schematic description of test case 1.0.

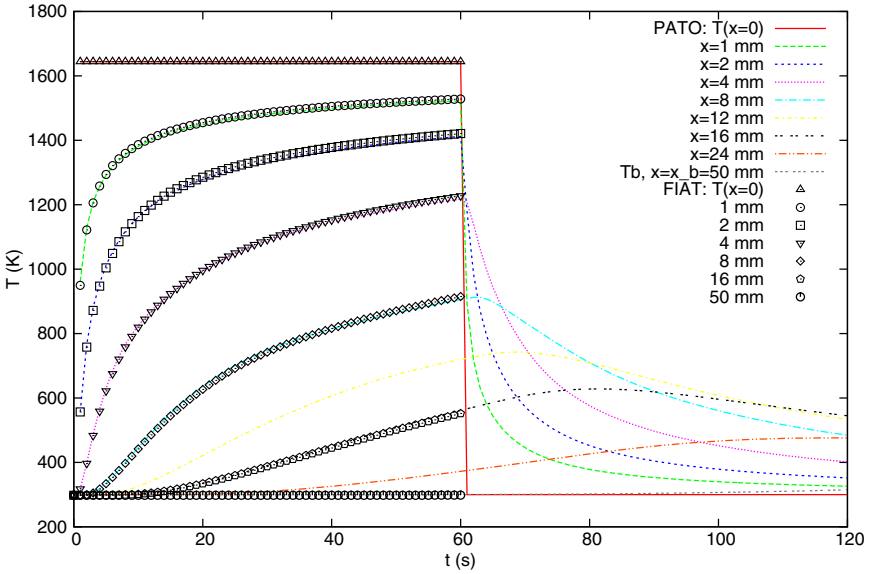

Fig. 10 Test case 1.0: Comparison of thermal response between PATO/PAM_2 and FIAT.

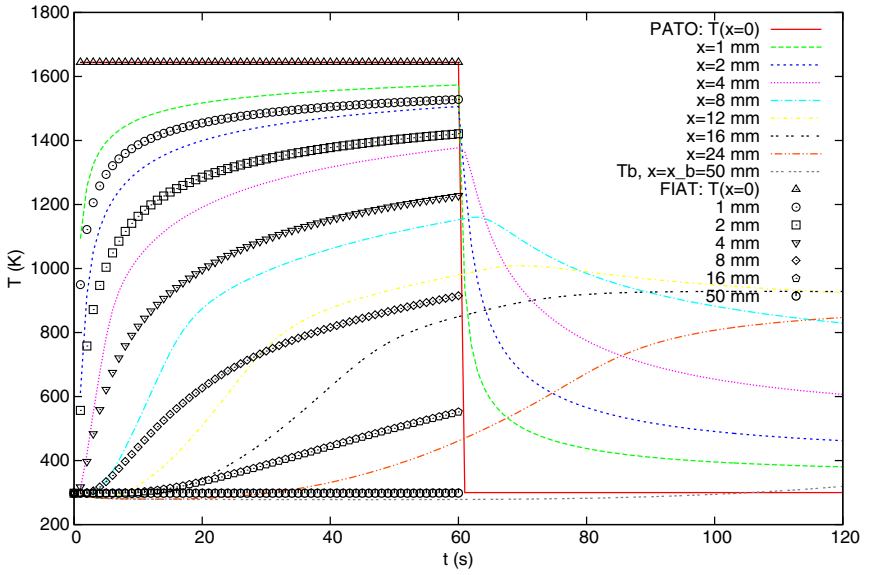

Fig. 11 Test case 1.0: Comparison of thermal response between PATO/PAM_3 and FIAT.

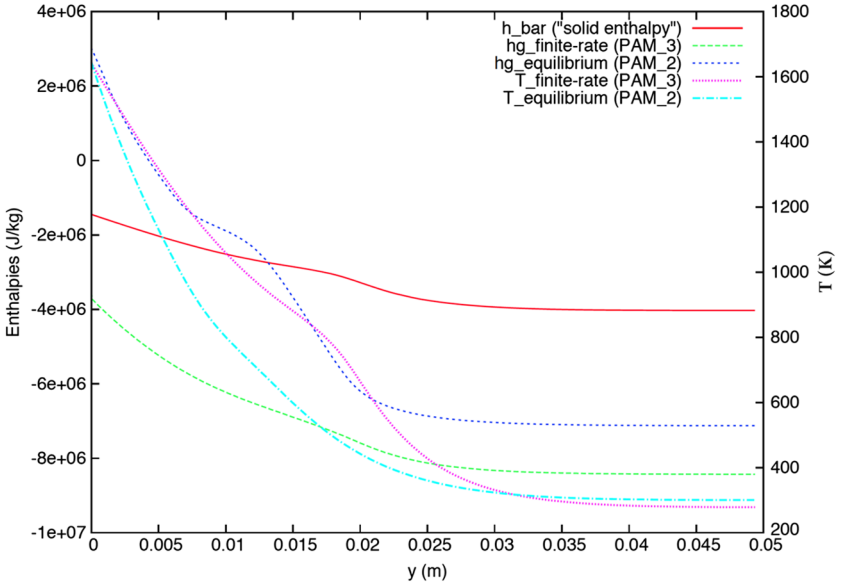

Fig. 12 Test case 1.0: Comparison of temperature and enthalpy profiles.

Downloaded by AIAA on August 11, 2014 | http://arc.aiaa.org | DOI: 10.2514/1.T4262

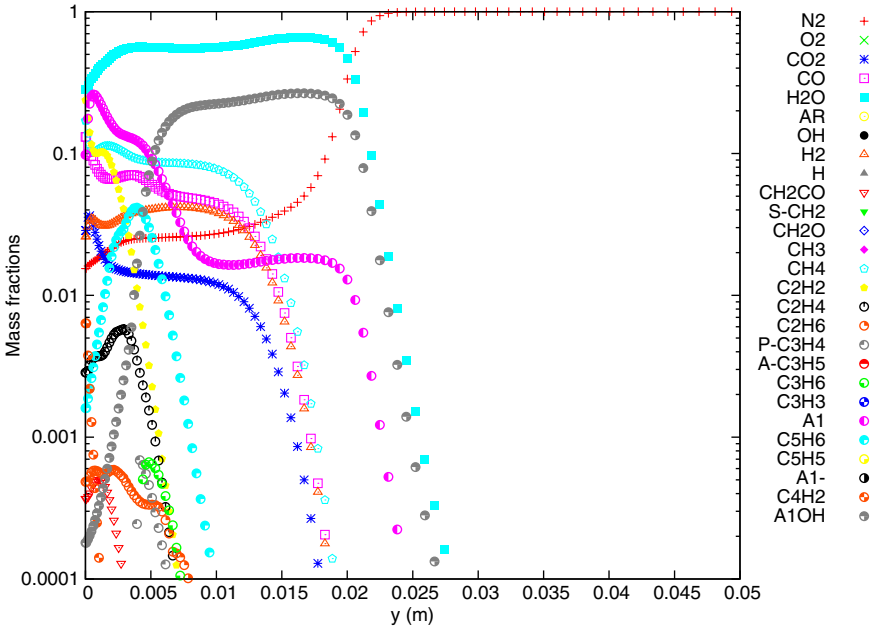

Fig. 13 Test case 1.0: PATO/PAM_3, Blanquart 22 species, with diffusion neglected.

VI. Conclusions

A volume-averaged derivation of a high-fidelity type 3 model and its associated boundary conditions have been presented. The proposed type 3 mathematical framework degenerates in state-of-the-art type 1 and type 2 models under the same physical hypotheses. This layered structure presents a remarkable advantage because new modules can easily and rigorously be compared to heritage models.

PATO is composed of two types of modules, a global analysis module and an elementary analysis module. The global analysis module may be used to run a full ablative material response with an applied/macroscopic scale point of view. The PAM module is an implementation of type 2 (PAM_2) and type 3 (PAM_3) material response models. Any physically correct variation between these two models can be run when selecting the right model options.

The elementary analysis module may be used to study specific fundamental aspects with a detailed/microscopic scale point of view. The COACO module is specifically developed to analyze carbon oxidation experiments and extract intrinsic reaction rates of carbon fibers. It is also used to test and validate volume-averaged fiber oxidation models needed for PAM_3.

Elementary analysis and global analysis applications have been proposed. They show how PATO complements the capabilities of current production codes. The elementary modules bring some insight into very specific problems, as illustrated here with the case of FiberForm oxidation. The global modules aim to compare different levels of modeling, and may be used to validate or invalidate hypotheses used in production codes. We have shown that neglecting Darcian effects is acceptable for simple unidimensional cases, but becomes incorrect for 3-D cases. A first analysis of finite rate chemistry effects in low-density carbon/phenolic materials has been carried out using literature finite rate chemistry data. Modeling accurately finite rate chemistry effects is critical for a correct prediction of the temperature profile in the sample and for the prediction of the gas species injected in the boundary layer.

PATO is available for worldwide academic release with some restrictions. The copyright is owned by NASA. Please contact the authors for more information.

Acknowledgments

This research was originally funded by NASA's Fundamental Aeronautic Program Hypersonics Nasa Research Announcement (NRA) grant NNX12AG47A. It is currently supported by the Space Technology Research Grants Program. The authors would like to thank G. Blanquart (Caltech) for providing a preliminary reduced mechanism of his combustion database. H. Jasak, H. Rusche, and Z. Tukovic are gratefully acknowledged for their interest in PATO and for their guidance during the second OpenFoam summer school (Numerical Modeling of Coupled Problems in Applied Physics with OpenFoam, Faculty of Mechanical Engineering and Naval Architecture, Zagreb, Croatia; 02–15 September 2009).

References

[1] Moyer, C. B., and Rindal, R. A., "An Analysis of the Coupled Chemically Reacting Boundary Layer and Charring Ablator: Part II," NASA CR, Vol. 1061, 1968, pp. 1–168.

[2] Sykes, G. F., "Decomposition Characteristics of a Char-Forming Phenolic Polymer Used for Ablative Composites," NASA TN, Vol. D-3810, 1967, pp. 1–20.

[3] Trick, K. A., and Saliba, T. E., "Mechanisms of the Pyrolysis of Phenolic Resin in a Carbon/Phenolic Composite," *Carbon*, Vol. 33, No. 11, 1995, pp. 1509–1515. doi:10.1016/0008-6223(95)00092-R

[4] Trick, K. A., Saliba, T. E., and Sandhu, S. S., "A Kinetic Model of the Pyrolysis of Phenolic Resin in a Carbon/Phenolic Composite," *Carbon*, Vol. 35, No. 3, 1997, pp. 393–401. doi:10.1016/S0008-6223(97)89610-8

[5] Lachaud, J., Cozmuta, I., and Mansour, N. N., "Multiscale Approach to Ablation Modeling of Phenolic Impregnated Carbon Ablators," *Journal of Spacecraft and Rockets*, Vol. 47, No. 6, 2010, pp. 910–921. doi:10.2514/1.42681

[6] Lachaud, J., and Mansour, N. N., "Microscopic Scale Simulation of the Ablation of Fibrous Materials," AIAA Paper 2010-984, 2010.

[7] Whitaker, S., *The Method of Volume Averaging*, Kluwer, Dordrecht, The Netherlands, 1999, pp. 1–179.

[8] Lachaud, J., Mansour, N. N., Ceballos, A., Pejakovic, D., Zhang, L., and Marschall, J., "Validation of a Volume-Averaged Fiber-Scale Model for the Oxidation of a Carbon-Fiber Preform," AIAA Paper 2011-2223, 2011.

[9] Lachaud, J., Magin, T., Cozmuta, I., and Mansour, N. N., "A Short Review of Ablative Material Response Models and Simulation Tools," *7th Aerothermodynamics Symposium*, European Space Agency, Noordwijk, The Netherlands, May 2011, pp. 1–8.

[10] Kendall, R. M., Bartlett, E. P., Rindal, R. A., and Moyer, C. B., "An Analysis of the Coupled Chemically Reacting Boundary Layer and Charring Ablator: Part I," NASA CR, Vol. 1060, 1968, pp. 1–96.

[11] Goldstein, H. W., "Pyrolysis Kinetics of Nylon 6-6, Phenolic Resin, and Their Composites," *Journal of Macromolecular Science, Part A*, Vol. 3, No. 4, 1969, pp. 649–673. doi:10.1080/10601326908053834

Downloaded by AIAA on August 11, 2014 | http://arc.aiaa.org | DOI: 10.2514/1.T4262

[12] Mansour, N. N., Lachaud, J., Magin, T. E., de Muelenaere, J., and Chen, Y. K., "High-Fidelity Charring Ablator Thermal Response Model," AIAA Paper 2011-3124, 2011.

[13] Ladacki, M., Hamilton, J. V., and Cohz, S., "Heat of Pyrolysis of Resin in Silica Phenolic Ablator," *AIAA Journal*, Vol. 4, No. 10, 1966, pp. 1798–1802. doi:10.2514/3.3699

[14] Laub, B., "High-Fidelity Model," *Tutorial on Ablative TPS*, Second International Planetary Probe Workshop, NASA Ames Research Center, Moffett Field, Aug. 2004, pp. 1–11.

[15] Blanquart, G., Pepiot-Desjardins, P., and Pitsch, H., "Chemical Mechanism for High Temperature Combustion Engine Relevent Fuels with Emphasis on Soot Precursors," *Combustion and Flame*, Vol. 156, No. 3, 2009, pp. 588–607.

[16] Panerai, F., Martin, A., Mansour, N. N., Sepka, S. A., and Lachaud, J., "Flow-Tube Oxidation Experiments on the Carbon Preform of PICA," AIAA Paper 2013-2769, 2013.

[17] Mansour, N. N., Panerai, F., Martin, A., Parkinson, D. Y., MacDowell, A., Fast, T., Vignoles, G. L., and Lachaud, J., "A New Approach to Light-Weight Ablators Analysis: From Micro-Tomography Measurements to Statistical Analysis and Modeling," AIAA Paper 2013-2768, 2013.

[18] Tran, H. K., Johnson, C. E., Rasky, D. J., Hui, F. C. L., Hsu, M. T., Chen, T., Chen, Y. K., Paragas, D., and Kobayashi, L., "Phenolic Impregnated Carbon Ablators (PICA) as Thermal Protection Systems for Discovery Missions," NASA TM-TR-110440, 1997, pp. 1–70.

[19] Marschall, J., and Milos, F. S., "Gas Permeability of Rigid Fibrous Refractory Insulations," *Journal of Thermophysics and Heat Transfer*, Vol. 12, No. 4, 1998, pp. 528–535. doi:10.2514/2.6372

[20] Puiroux, N., Prat, M., and Quintard, M., "Non-Equilibrium Theories for Macroscale Heat Transfer: Ablative Composite Layer System," *International Journal of Thermal Sciences*, Vol. 43, No. 6, 2004, pp. 541–554. doi:10.1016/j.ijthermalsci.2003.11.004

[21] van Eekelen, T., and Lachaud, J., "Radiation Heat-Transfer Model for the Ablation Zone of Low-Density Carbon-Resin Composites," AIAA Paper 2010-4904, 2010.

[22] van Eekelen, T., and Lachaud, J., "Numerical Validation of an Effective Radiation Heat Transfer Model for Fiber Preforms," *Journal of Spacecraft and Rockets*, Vol. 48, No. 3, 2011, pp. 534–537. doi:10.2514/1.51865

[23] Ene, H. J., and Sanchez-Palencia, E., "On Thermal Equation for Flow in Porous Media," *International Journal of Engineering Science*, Vol. 20, No. 5, 1982, pp. 623–630. doi:10.1016/0020-7225(82)90116-1

[24] Chen, Y. K., and Milos, F. S., "Ablation and Thermal Response Program for Spacecraft Heatshield Analysis," *Journal of Spacecraft and Rockets*, Vol. 36, No. 3, 1999, pp. 475–483. doi:10.2514/2.3469

[25] Moyer, C. B., and Wool, M. R., "Aerotherm Equilibrium Surface Thermochemistry Computer Program," Ver. 3, TR, Aerotherm, AD875385, April 1970.

[26] Lachaud, J., Martin, A., Cozmuta, I., and Laub, B., "Ablation Workshop Test Case," Ver. 1.1, Feb. 2011; Schmisseur, J., *4th Ablation Workshop*, Albuquerque, NM, March 2011.

[27] Lachaud, J., Martin, A., van Eekelen, T., and Cozmuta, I., "Ablation Test-Case Series #2," Ver. 2.8, Jan. 2011, p. 8; Martin, A., *5th Ablation Workshop*, Lexington, KY, Feb.–March 2011.

[28] van Eekelen, T., Martin, A., Lachaud, J., and Cozmuta, I., "Ablation Test-Case Series #3," Ver. 1.3, Nov. 2012; Martin, A., *5th Ablation Workshop*, Lexington, KY, Feb.–March 2012.

[29] Martin, A., and Boyd, I., "Simulation of Pyrolysis Gas within a Thermal Protection System," AIAA Paper 2008-3805, 2008.

[30] van Eekelen, T., Bouilly, J. M., Hudrisier, S., Dupillier, J. M., and Aspa, Y., "Design and Numerical Modelling of Charring Material Ablators for Re-Entry Applications," *Proceedings of the Sixth European Workshop on Thermal Protection Systems and Hot Structures*, European Space Agency, Noordwijk, The Netherlands, 2009, pp. 1–8.

Downloaded by AIAA on August 11, 2014 | http://arc.aiaa.org | DOI: 10.2514/1.T4262